

Tuning the quantum tunneling and quantum information properties among the trion states in coupled quantum dots

Y.B. Wen, W.X. Yan*

*Department of Physics, College of Physics and Electronics,
Shanxi University, Taiyuan, 030006, People's republic of China*

Abstract

Quantum transition and information properties of the Coulomb coupled trion (electron-electron-hole) in the double quantum dots under the influence of the time-dependent electric field have been studied. Tuning the Hubbard interaction strength amongst the states of electron-hole complexes and the parameters of the ac field, two strikingly different kinds of approximate qubit can be constructed within the eight trion states. The similarity and difference between the electron dynamic entanglement and overlapping of the wavefunction with the Bell state have been elucidated through analyzing these two kinds of qubit.

PACS numbers: 03.65.Ud, 73.23.-b, 78.67.Hc

arXiv:0804.4513v1 [quant-ph] 29 Apr 2008

* To whom correspondence should be addressed, E-mail: yanwxu@yahoo.com.cn

I. INTRODUCTION

The electronic transport phenomena in the quantum dots have been enriched by the introduction of the time-dependent driving external fields¹, partly due to the sidebands created by the harmonic fields, and these sidebands open additional more channels for the tunneling of the interacting electrons. More intriguing effect is the dynamic localization produced by the harmonic field, which control the electron to locate one of the states permanently or in a relatively long duration^{2,3,4,5,6,7,8,9,10}. The proper choice of the external harmonic field parameters can compensate the inadequacy of the artificial engineered nanostructures, and provides more possibilities to manipulate the electronic and transport properties of the electrons. Since the pioneering works of Loss and Divincenzo¹¹, the interacting electrons in the quantum dots have become one of the entities in the realization of solid state quantum computation. Besides taking the electron as the quantum information processing candidate, exciton^{6,12} and even charged exciton (trions)^{13,14,15,16} have been proposed as the candidates for the quantum information^{17,18,19,21}.

The two interacting electrons in coupled quantum dots have been studied by many authors, where dynamic localization and delocalization have been found^{3,4,7}, and possibility for the generation of maximum Bell state has been discussed⁷. Hubbard-like interacting excitons in the coupled quantum dots driven by harmonic field have been analyzed and entanglement has been realized^{6,12}. In a single quantum dot, manipulation of the spin of the Λ system consisting of the spin up/down states and trion state is performed by Economou and coauthors^{20,22}, where rotation of spin is realized through an optical way, providing an alternative way in controlling spin for quantum information processing. In our work, we study the dynamics of the electron-trion X^- in the coupled quantum dots, trion states in our model can be formed in either the same quantum dot or spatially-separated dots. The manipulation of the transition dynamics among the trion states has been made through tuning both the Coulombic interactions among the electron-hole interaction and parameters from the harmonic fields. In the Floquet picture, by resolving the special crossing points in quasienergies of the system^{3,7,10}, the resonant tunneling/Rabi flopping within the different trion states can be realized. Particular interesting phenomenon lies in the fact that the trion is capable of oscillating in the partial states of the all trion states for a long duration of time, while the tunneling to the other states becomes forbidden. In these various allowed-forbidden

configuration, two different kinds of quantum qubit have been constructed, the overlapping of the wavefunction with the maximum Bell state and the concurrence describing the electron entanglement have been compared and discussed. The so-called *electron entanglement dynamic single-slit* and *double-slit*²³ have been introduced to describe the similarity and difference between the overlapping and entanglement.

Our work is organized as follows, the model together with the brief description of the quasienergies and associated dynamics is presented in section II; The quantum information properties including the generation of qubit and dynamic electron entanglement are given in the Section III, section IV concludes our work.

II. THE MODEL AND TUNNELING DYNAMICS

To describe the electron-trion X^- in the coupled quantum dots, we introduce two quantum dots system whose energy-level detuning for both the electron and hole is neglected. In order for simplicity, The single-level approximation for both the electron and hole is adopted, that is to say, the harmonic driving field frequency ω is assumed to be much lower than the energy spacing between the single-particle ground state level and the first excited state level. If the tunneling rate in the QD systems is much larger than the electron-hole recombination rate and the electron-phonon interaction is neglected^{24,25}, Hubbard on-site interaction among electron and hole carriers can be employed, thus the Hamiltonian can be written as,

$$\begin{aligned} \mathcal{H}(t) = & \sum_{i,\ell,\sigma} \epsilon_{i,\ell,\sigma} d_{i,\ell,\sigma}^\dagger d_{i,\ell,\sigma} + \sum_i W_{i,\sigma} \left(d_{i,L,\sigma}^\dagger d_{i,R,\sigma} + h.c. \right) + \sum_{i \neq j, \sigma, \sigma} \frac{U_{ij,\sigma,\sigma}}{2} (n_{i,L,\sigma} n_{j,L,\sigma} + n_{i,R,\sigma} n_{j,R,\sigma}) \\ & + \sum_{i \neq j, \sigma, \sigma} \frac{V_{ij,\sigma,\sigma}}{2} (n_{i,L,\sigma} n_{j,R,\sigma} + n_{i,R,\sigma} n_{j,L,\sigma}) , \end{aligned} \quad (1)$$

where $d_{i,\ell,\sigma}^\dagger$ indicates creating an electron (hole) i in the ℓ -side (ℓ =left (right)) dot, and $d_{i,\ell,\sigma}$, annihilating an electron (hole) i in the ℓ -side (ℓ =left (right)) dot. $W_{i,\sigma}$ is the hopping parameter of electron (hole) between the two dots. $U_{ij,\sigma,\sigma}$ and $V_{ij,\sigma,\sigma}$ denote the intra-dot and inter-dot Coulombic interaction among the carriers respectively. $n_{i,\ell,\sigma}$ is the number of electrons or hole in the left (right) dot. When the QDs are biased by a harmonic field, their energy levels will be shifted as follows, $\epsilon_{i,\sigma}^\mp(t) = \epsilon_{i,\sigma}^0 \mp \frac{\phi}{2} \cos(\omega t)$, where the ϕ is the potential proportional to the product of amplitude of the harmonic field and spacing between the

QD. The electron-trion states can be described as follows in terms of the many-particle basis $d_{i_1, \ell_1, \sigma_1}^\dagger d_{i_2, \ell_2, \sigma_2}^\dagger d_{i_3, \ell_3, \sigma_3}^\dagger |0\rangle$, where i, ℓ, σ with the subscripts represent the electron/hole, left/right, spin up/down respectively. There are 32 states all together, while only eight states survive after taking account of the above assumptions. These eight X^- states can be represented as the ket states: $|e\bar{e}h\rangle$, where the spin-up, spin-down electrons and hole are arranged from the left to the right respectively in the ket. By further introducing the number 0 and 1 to indicate whether the carriers appear in the left or right QDs, the 8 electron-trion states can be written as: $|0\bar{0}0\rangle, |0\bar{0}1\rangle, |0\bar{1}0\rangle, |0\bar{1}1\rangle, |1\bar{0}0\rangle, |1\bar{0}1\rangle, |1\bar{1}0\rangle, |1\bar{1}1\rangle$ (denoted as: $|\varphi_\alpha\rangle, (\alpha = 1, 2, \dots, 8)$). Using these basis states, the corresponding Hamiltonian can be obtained in a matrix form as,

$$\mathcal{H}(t) = \begin{pmatrix} -\frac{3}{2}\mathcal{F}(t) & W_h & W_{2e} & 0 & W_e & 0 & 0 & 0 \\ W_h & 2\mathcal{U} - \frac{1}{2}\mathcal{F}(t) & 0 & W_{2e} & 0 & W_e & 0 & 0 \\ W_{2e} & 0 & -\frac{1}{2}\mathcal{F}(t) & W_h & 0 & 0 & W_e & 0 \\ 0 & W_{2e} & W_h & \frac{1}{2}\mathcal{F}(t) & 0 & 0 & 0 & W_e \\ W_e & 0 & 0 & 0 & -\frac{1}{2}\mathcal{F}(t) & W_h & W_{2e} & 0 \\ 0 & W_e & 0 & 0 & W_h & \frac{1}{2}\mathcal{F}(t) & 0 & W_{2e} \\ 0 & 0 & W_e & 0 & W_{2e} & 0 & 2\mathcal{U} + \frac{1}{2}\mathcal{F}(t) & W_h \\ 0 & 0 & 0 & W_e & 0 & W_{2e} & W_h & \frac{1}{2}\mathcal{F}(t) \end{pmatrix}, \quad (2)$$

where the gauge transformation $\exp(-i(2\epsilon_{e\sigma} + \epsilon_{h\sigma} + U_{1h\sigma}))$ has been performed to eliminate the common term in the diagonal part of the Hamiltonian; the interaction strength $|\mathcal{U}_1|$ and $|V_1|$ among the carriers in the intra-dot and inter-dot are assumed respectively, without loss of generality. In the above effective Hamiltonian, $\mathcal{F}(t) = \phi \cos(\omega t)$, and $\mathcal{U} = -|\mathcal{U}_1| + |V_1|$. The above system can not be solved in an exact way due to the non-commutativity of the Hamiltonian at different times. However Floquet theorem provides a solution clue to the time-periodic system: $|\Psi_{\alpha,m}(t)\rangle = \exp(-i\varepsilon_{\alpha,m}t) |u_{\alpha,m}(t)\rangle$. The Floquet state $|u_{\alpha,m}(t)\rangle$ satisfies the following alternative Schrödinger equation,

$$\left(\mathcal{H}(t) - i \frac{\partial}{\partial t} \right) |u_{\alpha,m}\rangle = \varepsilon_{\alpha,m} |u_{\alpha,m}\rangle, \quad (3)$$

where the quasienergy $\varepsilon_{\alpha,m}$ is restricted in the first Brillouin zone $[-\frac{\omega}{2}, \frac{\omega}{2}]$. The merit of the introduction of the time-dependent external fields lies in that the dynamics can be tuned to the regime of the interest. While from the generalized parity symmetry point of view, the

subsequent Floquet states can be classified into even parity or odd parity states, the quasienergies belonging to the different and same symmetry may develop into exact crossings and avoided crossings respectively^{1,27}. By choosing the parameters corresponding to these special points, the intriguing quantum information properties will be disclosed, which have been reported in the section III.

The changing behavior of the quasienergies and minimum propagator probability $P_\alpha^{min}(\equiv \min(|c_\alpha(t_j)|^2), j = 1, 2, \dots, N$, with $t_N = 30T(\alpha = 1, 2)$) with the driving potential ϕ has been illustrated in Fig.1, where we use the parameters: $W_e = W_{2e} = 1.0, W_h = 0.6, \omega = 2.0$, the Coulombic interaction difference \mathcal{U} has been taken -1 . The enhancement of the Coulombic interaction \mathcal{U} induces asymmetry of quasienergies about the horizontal axis. Closer inspection of the Hamiltonian in Eq.(2) reveals that the present system can be viewed as the two coupled dot arrays with four dots(states) in each array, and hopping term between the array is W_e (see the Fig.2). This explains why the quasienergies are split into two parts. Also in Fig.1, the survival probabilities P_1^{min} and P_2^{min} have been depicted, where the initial conditions have been chosen as $c_1(0) = 1.0$ or $c_2(0) = 1.0$ respectively. It is interesting that the peaks for P_1^{min} and P_2^{min} appear in different exact crossing points of the quasienergies. All these show that the states: $|\varphi_1\rangle$ and $|\varphi_2\rangle$ contain different generalized symmetry component of Floquet functions^{26,27}. Another interesting phenomenon is that P_2^{min} have two neighboring peaks, forming bistable structures which result from the closely-spacing exact crossings in the quasienergies.

III. THE GENERATION OF QUBIT AND DYNAMIC ELECTRON ENTANGLEMENT

Rajagopal and Rendell analyzed eight states from triple-qubit, where robust and fragile entanglement are classified²⁸. Although there are eight states in our system, these eight states from three non-identical particles can not be mapped onto triple-qubit eight states, since there exists spatial freedom as well as spin freedom in our system. The states $|0\bar{0}0\rangle$ and $|1\bar{1}1\rangle$ represent that the trion stays in the same QD, while the other states belong to the spatially separated trion states.

Even if there is no obvious qubit in our system, we can tune the system parameters and harmonic driving field to create the qubit. Fig.3 gives transition dynamics among the eight

trion states, where parameters used are: $\mathcal{U} = -20.0$, $W_h = 0.6$, $W_e = 1.7$, $\omega = 2.0$, $\phi = 24.6$. The driving potential ϕ is chosen to be around the avoided crossing point of the quasienergies. From the transition dynamics pattern in the figure, it can be clearly seen that the quantum transition nearly takes place among only three states: $|0\bar{0}0\rangle$, $|0\bar{1}0\rangle$, and $|1\bar{0}0\rangle$. Particularly interesting phenomenon lies in that the dynamics for $|0\bar{1}0\rangle$, and $|1\bar{0}0\rangle$ is highly equivalent in both the amplitude and phase. In this circumstance, $|0\bar{0}0\rangle$ together with the normalized linear combination state: $|\eta\rangle \equiv \frac{1}{\sqrt{2}}(|0\bar{1}0\rangle + |1\bar{0}0\rangle)$, can be esteemed as a spatial-separated qubit²⁹: $|\gamma\rangle \approx (c_1(t)|0\bar{0}0\rangle + c_3(t)|\eta\rangle)$.

Inspection of the configuration of the eight trion states indicates that electron dynamic entanglement can be realized among the eight trion states from spatial degree of freedom. In order to measure the degree of the entanglement, we need to calculate the concurrence^{28,30} of the electron-electron density matrix, which is defined as,

$$\varrho_{ee} := \text{Tr}_h \varrho_{eeh} = \sum_1^{N_h} \left(\mathbf{I}_{ee} \otimes_h \langle \chi_j | \right) \varrho_{eeh} \left(\mathbf{I}_{ee} \otimes | \chi_j \rangle_h \right), \quad (4)$$

where Tr_h represents the partial trace over the hole basis $|\chi_j\rangle_h$; \otimes is the direct product and \mathbf{I}_{ee} is the 4×4 unit matrix. From the above equation, the electron-electron density matrix ϱ^{ee} can be evaluated to be

$$\varrho_{ee} = \begin{pmatrix} |c_1|^2 + |c_2|^2 & c_1 c_3^* + c_2 c_4^* & c_1 c_5^* + c_2 c_6^* & c_1 c_7^* + c_2 c_8^* \\ c_3 c_1^* + c_4 c_2^* & |c_3|^2 + |c_4|^2 & c_3 c_5^* + c_4 c_6^* & c_3 c_7^* + c_4 c_8^* \\ c_5 c_1^* + c_6 c_2^* & c_5 c_3^* + c_6 c_4^* & |c_5|^2 + |c_6|^2 & c_5 c_7^* + c_6 c_8^* \\ c_7 c_1^* + c_8 c_2^* & c_7 c_3^* + c_8 c_4^* & c_7 c_5^* + c_8 c_6^* & |c_7|^2 + |c_8|^2 \end{pmatrix} \quad (5)$$

The other matrix $\tilde{\varrho}_{ee}$, necessary for the calculation of the concurrence can be constructed through the following way,

$$\begin{aligned} \tilde{\varrho}_{ee} &= (\sigma_y \otimes \sigma_y) \varrho_{ee}^* (\sigma_y \otimes \sigma_y) \\ &= \begin{pmatrix} |c_7|^2 + |c_8|^2 & -(c_2 c_5^* + c_8 c_6^*) & -(c_7 c_3^* + c_8 c_4^*) & c_7 c_1^* + c_8 c_2^* \\ -(c_5 c_7^* + c_6 c_8^*) & |c_5|^2 + |c_6|^2 & c_5 c_3^* + c_6 c_4^* & -(c_5^* c_1 + c_6 c_2^*) \\ -(c_3 c_7^* + c_4 c_8^*) & c_3 c_5^* + c_4 c_6^* & |c_3|^2 + |c_4|^2 & -(c_3^* c_1 + c_4 c_2^*) \\ c_1 c_7^* + c_2 c_8^* & -(c_1 c_5^* + c_2 c_6^*) & -(c_1 c_3^* + c_2 c_4^*) & |c_1|^2 + |c_2|^2 \end{pmatrix}. \quad (6) \end{aligned}$$

The procedure for the calculation of the concurrence is to find the eigenvalues of the Hermitian matrix $\sqrt{\varrho \tilde{\varrho} \varrho}$. The concurrence is obtained as $C_{ee} = \max\{\lambda_1 - \lambda_2 - \lambda_3 - \lambda_4, 0\}$, where

λ_i ($i = 1, 2, 3, 4$) are the square roots of the eigenvalues of the matrix $\sqrt{\sqrt{\rho}\tilde{\rho}\sqrt{\rho}}$ arranged in decreasing order^{28,30}.

In the case of Fig.3, let us focus on the electron entanglement of the state $|0\bar{1}0\rangle$ and $|1\bar{0}0\rangle$, the non-vanishing $c_i(t)$ are $c_1(t)$, $c_3(t)$, $c_5(t)$ with the other $c_i(t)$ ($i = 2, 4, 6, 7, 8$) almost vanishing, leading to

$$\rho_{\tilde{\rho}} \approx \begin{pmatrix} 0 & 2c_1^*c_3|c_5|^2 & 2c_1^*c_5|c_3|^2 & -2c_5c_3|c_1|^2 \\ 0 & 2|c_3|^2|c_5|^2 & 2c_3^*c_5|c_3|^2 & -2c_1^*c_5|c_3|^2 \\ 0 & 2c_5^*c_3|c_5|^2 & 2|c_3|^2|c_5|^2 & -2c_3^*c_1|c_5|^2 \\ 0 & 0 & 0 & 0 \end{pmatrix}, \quad (7)$$

whose eigenvalues can be evaluated to be $\{4|c_3|^2|c_5|^2, 0, 0, 0\}$. Hence, the concurrence $C_{ee}(t) = 2|c_3(t)||c_5(t)|$, which was depicted in the up panel of Fig.4. The overlapping of the state $|\psi(t)\rangle$ with the maximum-entangled Bell state $|\psi_{Bell}\rangle = \frac{1}{\sqrt{2}}(|0\bar{1}0\rangle + |1\bar{0}0\rangle)$, i.e., $\rho_1(t) = |\langle\psi(t)|\psi_{Bell}\rangle|^2 \approx (|c_3(t) + c_5(t)|^2)/2$ is given in the middle panel of the Fig.4, and the bottom panel gives both the curves for comparison. From the figures, it can be clearly seen that the occurrence oscillates with time and reach the maximum entanglement when the quenching of the trion state $|0\bar{0}0\rangle$ in the left QD occurs. Particularly, it is remarkable that the concurrence is coincident with the overlapping in the present case. This coincidence can be attributed to the fact that the propagator $c_3(t)$ is equal to $c_5(t)$, leading to $\rho_1(t) \approx |c_3(t) + c_5(t)|^2 = 2|c_3(t)||c_5(t)| \approx C_{ee}(t)$. The situation here can be pictorially described as the *electron entanglement dynamic single-slit*, where the maximum Bell state passes through the qubit $|\gamma\rangle \approx (c_1(t)|0\bar{0}0\rangle + c_3(t)|\eta\rangle)$. The qubit here only has a dynamic single-slit $c_3(t)|\eta\rangle$ (the other component of qubit $c_1(t)|0\bar{0}0\rangle$ is blind to the Bell state), which is the very reason why overlapping is equivalent to the concurrence.

The full dynamic entanglement of the electrons taking account of all propagators $c_i(t)$, ($i = 1, 2, \dots, 8$) is depicted in Fig. 5, where both the concurrence $C_{ee}(t)$ and overlapping $\rho_1(t)$ is given for comparison. The difference between the full concurrence and overlapping mainly results from the leaving out the tiny but non-vanishing propagator $c_7(t)$. The presence of the tiny propagator $c_7(t)$ induces the other entanglement: $\frac{1}{\sqrt{2}}(|0\bar{0}0\rangle + |1\bar{1}0\rangle)$. The full dynamic concurrence is composed of two sorts of entanglement $\frac{1}{\sqrt{2}}(|0\bar{1}0\rangle + |1\bar{0}0\rangle)$, and $\frac{1}{\sqrt{2}}(|0\bar{0}0\rangle + |1\bar{1}0\rangle)$, but the former one is much larger than the latter. This explains why the full concurrence is slightly larger than the overlapping (see the bottom panel of Fig.5).

Does the *dynamic double-slit* for the electron entanglement exist? As matter of fact, besides the above mentioned qubit, there exists other form of qubit which can be considered as electron entanglement dynamic double-slit, if we alter both the Coulombic interaction strength and harmonic driving field parameters in a proper way. The case is depicted in Fig.6, where the strong driving potential $\phi = 40.7$ are used, the other parameters used are the same as those in Fig.1. The transition dynamics shown in the figure is calculated with the initial condition: $(c_1(0), c_2(0), c_3(0), c_4(0), c_5(0), c_6(0), c_7(0), c_8(0)) = (1/\sqrt{2}, 0, 0, 0, 0, 0, 1/\sqrt{2}, 0)$. It is evident that the transition dynamics for $|0\bar{0}0\rangle, |1\bar{1}0\rangle$ is virtually the same, making transition to $|0\bar{0}1\rangle, |1\bar{1}1\rangle$ respectively in a nearly synchronous way. The outcome can be attributed to the fact that the strong driving force prevails over the attractive force between the electrons and hole, making the hole in one QD tunnel into the other QD. These four trion states are able to forming new approximate qubit: $|\delta\rangle \approx (c_1(t)|\alpha\rangle + c_2(t)|\beta\rangle)$, where $|\alpha\rangle = \frac{1}{\sqrt{2}}(|0\bar{0}0\rangle + |1\bar{1}0\rangle)$ and $|\beta\rangle = \frac{1}{\sqrt{2}}(|0\bar{0}1\rangle + |1\bar{1}1\rangle)$. The difference between the qubit $|\delta\rangle$ and the previously defined qubit $|\gamma\rangle$ lies in the different degree of spatial separation of the electrons within the two components of qubit. In the previously defined qubit $|\gamma\rangle$, only one electron populates in the different QD within the two components of qubit; while all the two electrons populate in different QD in the present qubit $|\delta\rangle$.

Through taking inner product with the Bell state $|\beta\rangle$, the probability $\rho_2(t) = |\langle\beta|\Psi(t)\rangle|^2$ for the system to stay in the Bell state $|\beta\rangle$ is given in the middle panel of Fig.7, where the up panel gives the concurrence $C_{ee}(t) \approx 2|c_2(t)||c_8(t)|$, when we force the propagator $c_1(t)$ and $c_7(t)$ to vanish. The bottom panel gives both concurrence and overlapping for comparison, where the envelope of the overlapping is almost coincident with the concurrence. But there is striking difference between the concurrence and overlapping, the pattern in the latter figure is irregular, forming many spikes. The reason behind this irregularity comes from the tiny phase difference between the two propagators $|c_2(t)|^2$, and $|c_8(t)|^2$, which are illustrated in the Fig.8. The quantum interference from these two probability terms leads to the shaping of the irregular pattern in Fig.7. Similar to Fig.7, Fig.9 gives the overlapping $\rho_3(t) = |\langle\alpha|\Psi(t)\rangle|^2$ and concurrence $C_{ee}(t) \approx 2|c_1(t)||c_7(t)|$ where both $c_2(t)$ and $c_8(t)$ have been set to vanish. The envelope of the overlapping matches the concurrence in a perfect way. As matter of fact, both Fig.7 and Fig.9 correspond to the case of shutting down one of the two dynamic slits $c_1(t)|\alpha\rangle$ and $c_2(t)|\beta\rangle$. It should be pointed out that the state of the hole play the role of picking out one of the two the Bell states $|\alpha\rangle$ or $|\beta\rangle$. This selecting

process corresponds to the overlapping of the wavefunction with state $|\alpha\rangle$ or $|\beta\rangle$.

When both the dynamic slit become transparent, the full concurrence can be approximately calculated as

$$C_{ee}(t) \approx \sqrt{A + \sqrt{BC}} \quad (8a)$$

$$A = \left[(|c_1(t)|^2 + |c_2(t)|^2) (|c_7(t)|^2 + |c_8(t)|^2) + |c_1^*(t)c_7(t) + c_2^*(t)c_8(t)|^2 \right] \quad (8b)$$

$$B = (|c_7(t) + c_8(t)|^2) \text{Re} (c_1^*(t)c_7(t) + c_2^*(t)c_8(t)) \quad (8c)$$

$$C = (|c_1(t) + c_2(t)|^2) \text{Re} (c_1^*(t)c_7(t) + c_2^*(t)c_8(t)) , \quad (8d)$$

where Re represents the real part. The exact numerical value of the full concurrence $C_{ee}(t)$ is plotted in the up panel of Fig.10, the bottom panel of the same figure gives $\rho_2(t)$, $\rho_3(t)$ and $C_{ee}(t)$ for comparison, where the full concurrence is coincident with the envelope of either $\rho_2(t)$ or $\rho_3(t)$ in different moment. The concurrence from dynamic double-slit does own different evolution behavior than the wavefunction does in quantum mechanics. In contrast to the usual double-slit, where the wavefunctions experience the prominent quantum interference, the terminology dynamic single-slit and double-slit here are for pictorial description since the entanglement interference here bears the striking different behavior than the usual double-slit wavefunction interference as illustrated in Fig.5 and Fig.10.

IV. CONCLUDING REMARK

We have investigated the coherent transition dynamics and explored the quantum information properties of the electron-trion X^- confined in two coupled quantum dots driven by an ac electric field. The transition dynamics among the eight trion states is controlled through the consideration of the symmetry of the Floquet states, which is embodied in the avoided crossing and exact crossing in the quasienergies spectrum. The tunneling dynamics among the eight trion states also depends sensitively on the difference of Coulombic interactions between the electrons and hole in the same QD and spatially-separated QD. Tuning the motion of the electrons and hole to evolve in partial states of the whole eight trion states, the allowed and forbidden trion states within the transition dynamics can be captured through which the two different kinds of the qubit can be constructed. From spatial degree of freedom, electron entanglement can be produced and the resulting concurrence has been given in both analytical and exact numerical results. The similarity and difference

between the concurrence and overlapping of the wavefunction with the maximum Bell state have been elucidated. Pictorially, one kind of qubit can be conceived as dynamic single-slit, while the other kind of qubit can be considered as the the dynamic double-slit for the electron entanglement.

Acknowledgments

This work is supported by the Shanxi Liuxue Foundation, and partly supported by Natural Science Foundation of China with No. 10475053.

-
- ¹ G. Platero, R. Aguado, Phys. Rep. **395**, 1 (2004) and references therein.
 - ² F. Grössmann, T. Dittrich, P. Jung, and P. Hänggi, Phys. Rev. Lett. **67**, 516 (1991).
 - ³ C. E. Creffield, Phys. Rev. B **67**, 165301 (2003).
 - ⁴ E. Paspalakis, Phys. Rev. B **67**, 233306 (2003).
 - ⁵ C. S. Liu, and B. K. Ma, Phys. Lett. A **315**, 301 (2003).
 - ⁶ Y.S. Liu, and H. Chen, Phys. Lett. A **324**, 235 (2004).
 - ⁷ P. Zhang, Q. K. Xue, X. G. Zhao, and X. C. Xie, Phys. Rev. A **66**, 022117 (2002).
 - ⁸ P. Zhang, X.G. Zhao, J. Phys.: Condens. Matter **12**, 2351 (2000).
 - ⁹ J. Danckwerts, K. J. Ahn, J. Föstner, and A. Knorr, Phys. Rev. B **73**, 165318 (2006).
 - ¹⁰ G.E. Murgida, D.A. Wisniacki, and P.I. Tamborenea, Phys. Rev. Lett. **99**, 036806 (2007).
 - ¹¹ D. Loss and D.P. DiVincenzo, Phys. Rev. A **57**, 120 (1998).
 - ¹² Luis G.G.V. Dias da Silva, J. M. Villas-Bôas, and S.E. Uolla, Phys. Rev. B **76**, 155306 (2007).
 - ¹³ For a short review on the physical properties of the trion, see E. Runge, *Solid State Physics*, **57**, 149 (Academic press) (2000).
 - ¹⁴ A. Esser, E. Runge, R. Zimmermann, and W. Langbein, Phys. Rev. B **62**, 8232 (2000).
 - ¹⁵ F.M. Peeters, C. Riva, and K. Varga, Few-Body Systems, **31**, 97 (2002).
 - ¹⁶ M. Combescot, O. Betbeder-Matibet, and F. Dubin Eur. Phys. J. B **42**, 63 (2004).
 - ¹⁷ A. Shabaev, Al. L. Efros, D. Gammon, and I.A. Merkulov, Phys. Rev. B **68**, 201305 (2003).
 - ¹⁸ Pochung Chen, C. Piermarocchi, L. J. Sham, D. Gammon, and D.G. Steel, Phys. Rev. B **69**, 75320 (2004).

- ¹⁹ S.E. Economou, and T.L. Reinecke, Phys. Rev. Lett. **99** 217401 (2007).
- ²⁰ M. Bayer, G. Ortner, A. Forchel, Y.B. Lyanda-Geller, T.L. Reinecke, P. Hawrylak, S. Fafard, and Z.R. Wasilewski, Phys. Rev. Lett. **90**, 086404 (2003).
- ²¹ J. R. Goldman, *Nuclear Spin detection and optical pumping in semiconductor quantum dots* PhD dissertation, (unpublished) (2005).
- ²² S. E. Economou, L.J. Sham, Yanwen Wu, and D.G. Steel, Phys. Rev. B **74**, 205415 (2006).
- ²³ The electron entanglement dynamic single slit and double slit are for pictorial and physical description, the former means that there is only one mechanisms contribution to the concurrence, while the latter contains two mechanisms.
- ²⁴ David M.-T. Kuo, and Yia-Chung Chang, Phys. Rev. B **72**, 085334 (2005).
- ²⁵ P. Hawrylak, Phys. Rev. B **60**, 5597 (1999).
- ²⁶ M. Holthaus, Z. Phys. B **89**, 251 (1992).
- ²⁷ T. Dittrich, P. Hänggi, G.-L. Ingold, B. Kramer, G. Schön, and W. Zwerger, *Quantum Transport and Dissipation*, chapter 5 (Wiley-VCH, Weinheim) (1998).
- ²⁸ A. K. Rajagopal, and R. W. Rendell, Phys. Rev. A **65**, 032328 (2002).
- ²⁹ R. Doll, M. Wubs, P. Hänggi, and S. Kohler, Europhys. Lett. **76**, 547 (2006).
- ³⁰ W. K. Wothers, Phys. Rev. Lett. **80**, 2245 (1998).

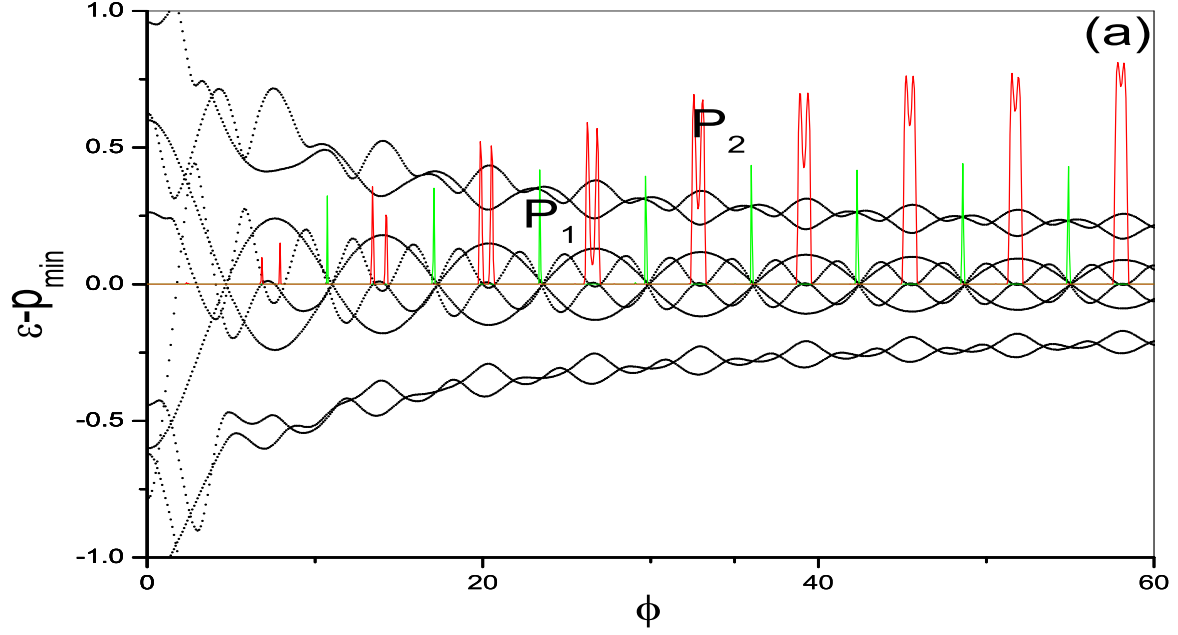


FIG. 1: Quasienergies ϵ and $P_\alpha^{min}(\phi)$, ($\alpha = 1, 2$) plotted as the external ac driving potential ϕ , the minimum propagator probabilities $P_\alpha^{min}(\phi)$ in a 30 periods time duration experience completely different tunneling behavior for $\alpha = 1$, and 2.

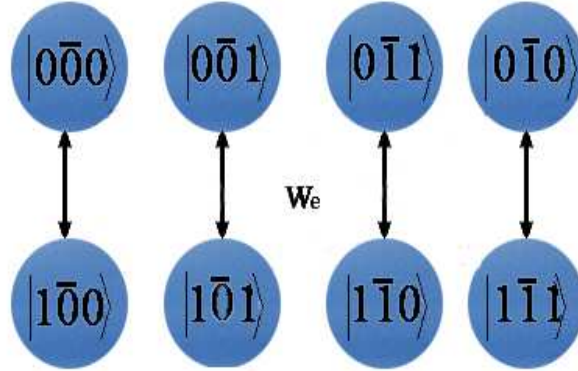


FIG. 2: The equivalent schematic picture of the Hamiltonian defined in Eq.(2), resembling the two arrays of single-level dots (states) coupled through the hopping term W_e .

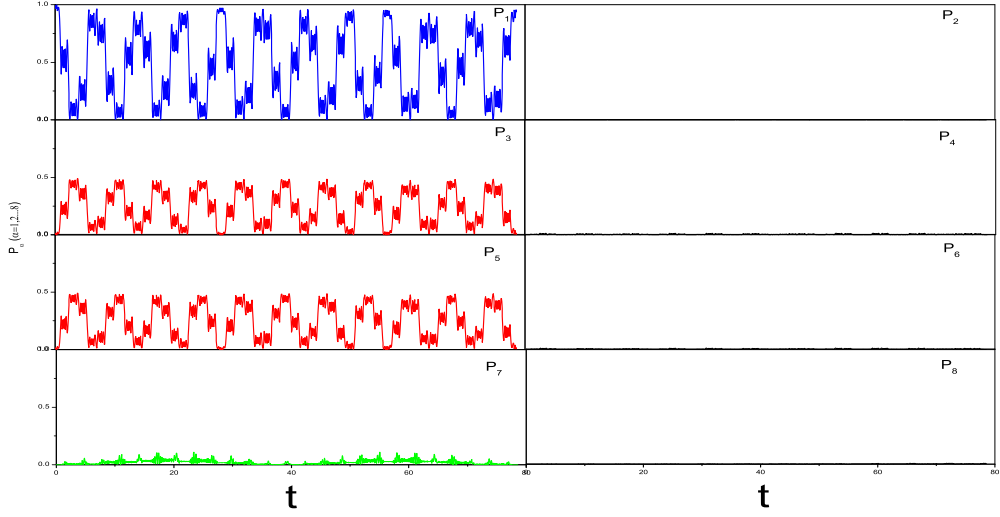


FIG. 3: The quantum transition dynamics among the eight trion states leading to the formation of the first kind of approximate dynamic qubit, the parameters used are declared in the text.

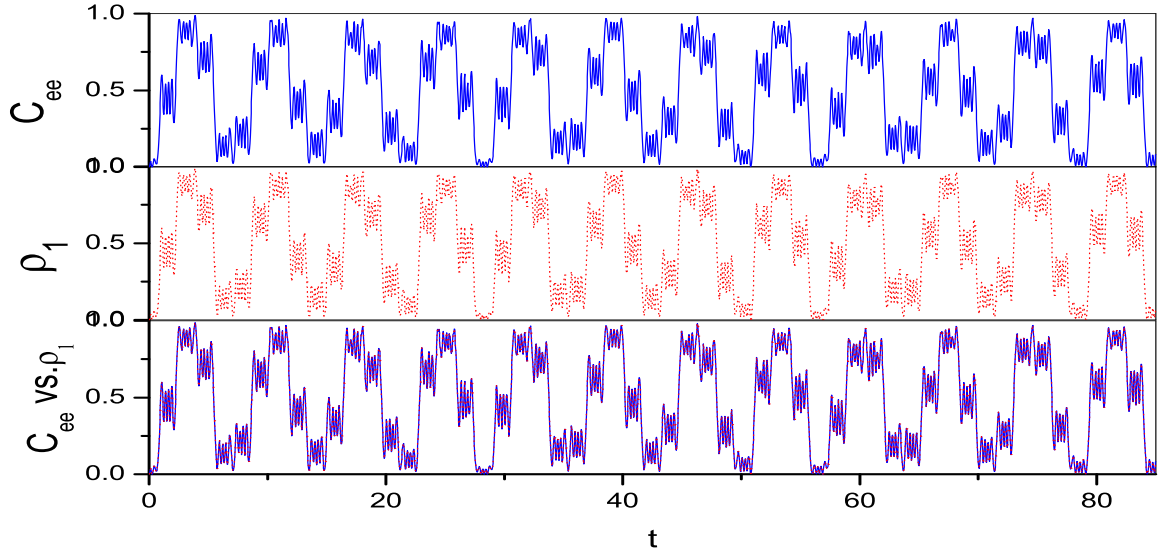


FIG. 4: The approximate concurrence calculated from the analytical expression $C_{ee}(t) = 2|c_3(t)||c_5(t)|$ and exact numerical overlapping of the wavefunction with the maximum Bell state, showing the consistency of the two quantity, the parameters used are the same as those in Fig.3.

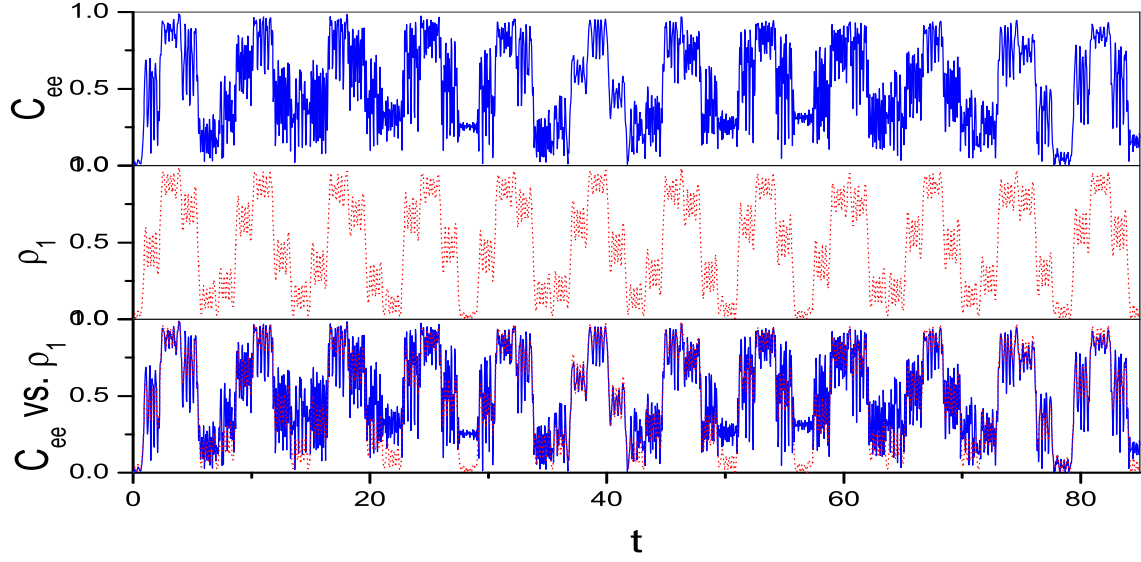


FIG. 5: The same as Fig.4, except that the concurrence is calculated from the exact numerical result taking account of all $c_i(t)$, ($i = 1, 2, \dots, 8$).

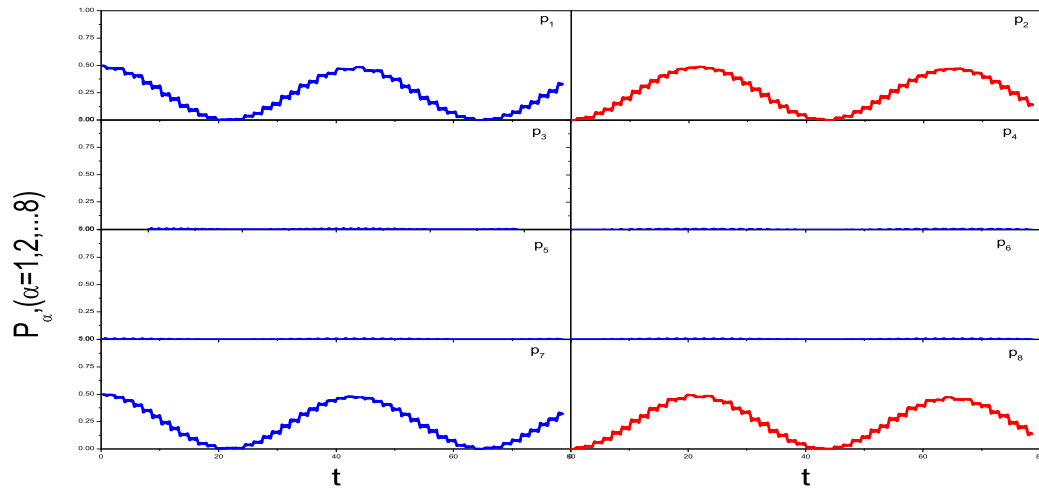


FIG. 6: The quantum transition dynamics among the eight trion states leading to the formation of the second kind of approximate dynamic qubit, the parameters used are declared in the text.

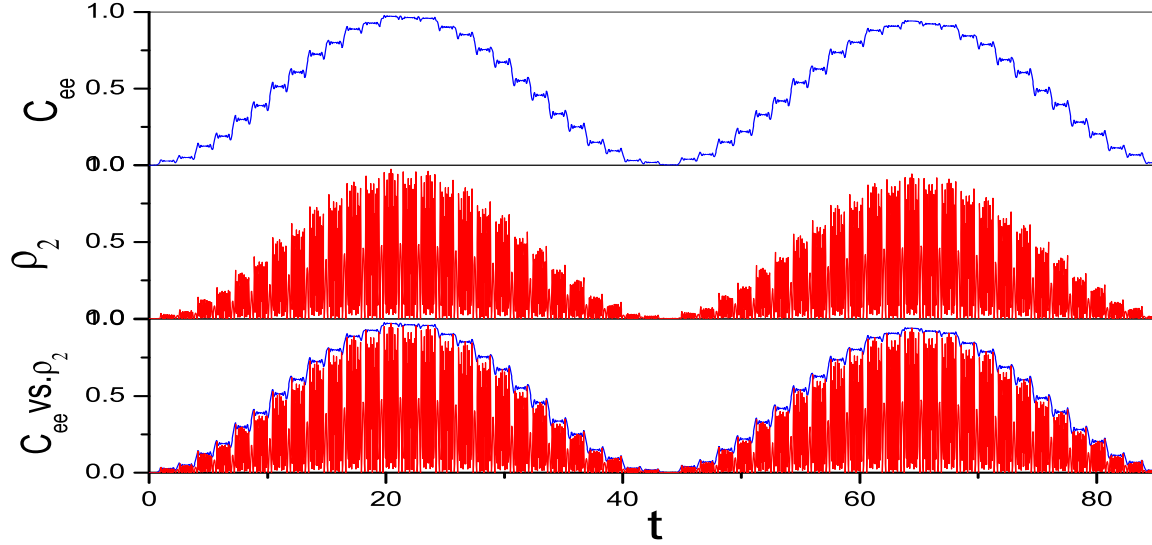


FIG. 7: The approximate concurrence calculated from $C_{ee} \approx 2|c_2(t)||c_8(t)|$ with $c_1(t)$ and $c_7(t)$ being set to vanish, and exact numerical overlapping of the wavefunction the maximum Bell state, the envelope of the overlapping is coincident with the concurrence.

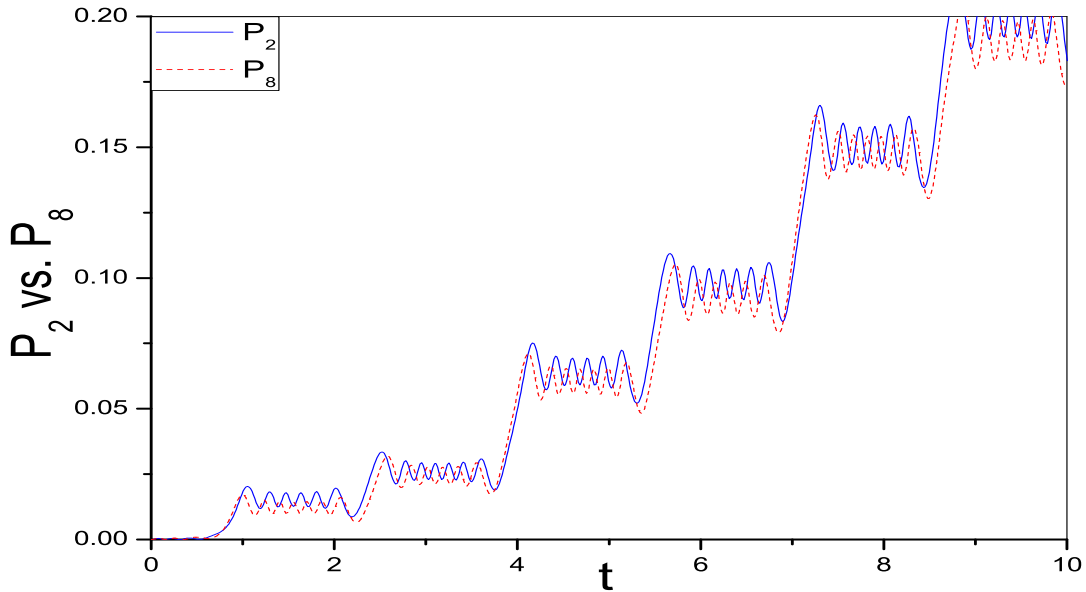


FIG. 8: The propagator $P_2 = |c_2(t)|^2$ plotted with blue solid line and $P_8 = |c_8(t)|^2$ plotted with red dashed line, showing the tiny phase difference between the two propagators probability, leading to the spikes of the overlapping in Fig.7.

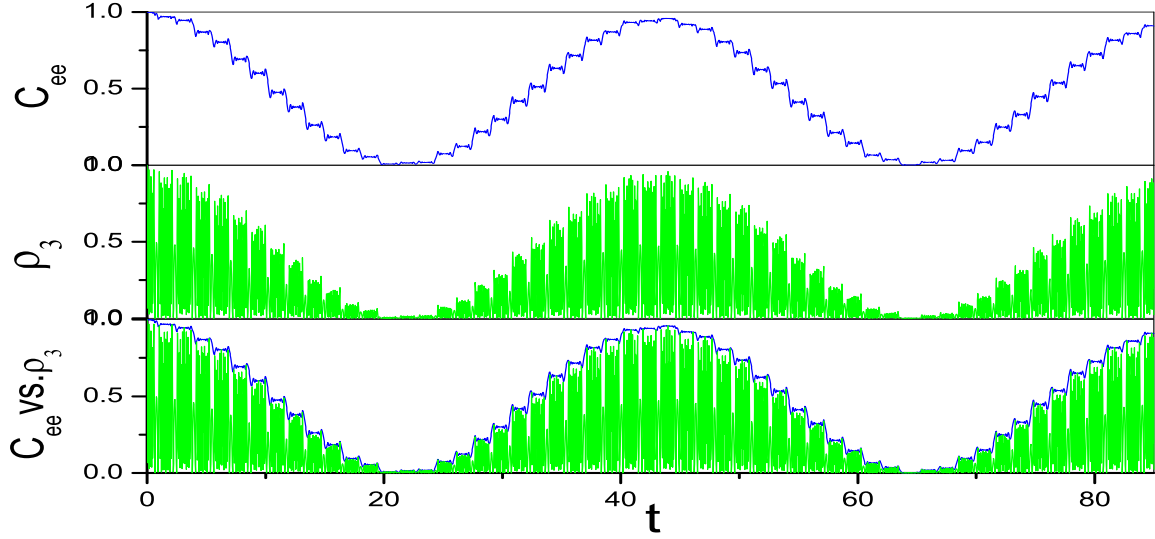


FIG. 9: The approximate concurrence calculated from $C_{ee} \approx 2|c_1(t)||c_7(t)|$ with $c_2(t)$ and $c_8(t)$ being set to vanish, and exact numerical overlapping of the wavefunction the maximum Bell state, the envelope of the overlapping is coincident with the concurrence.

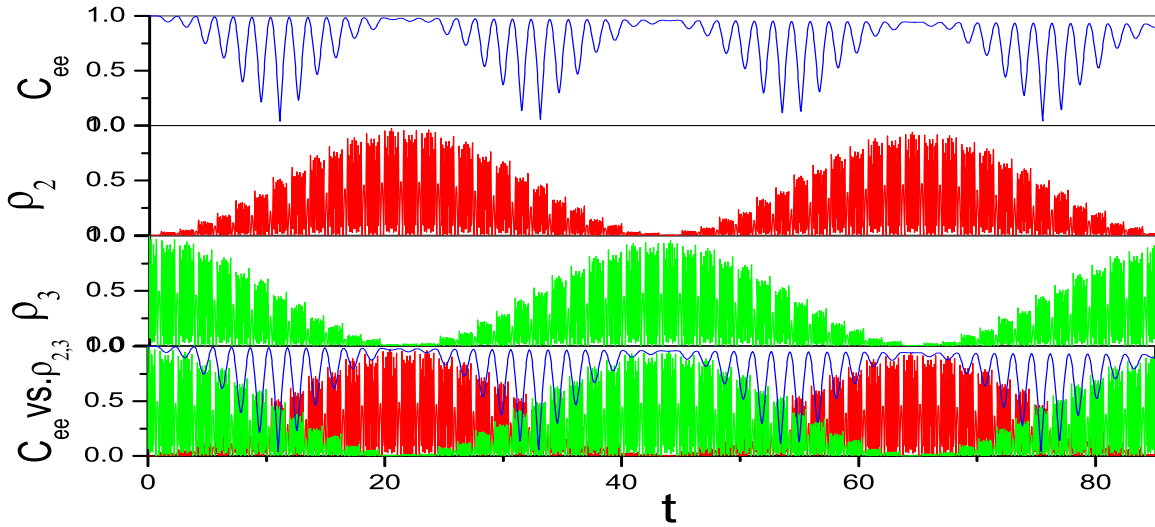


FIG. 10: The full concurrence calculated from the exact numerical result taking account of all $c_i(t)$, ($i = 1, 2, \dots, 8$) is plotted against the two overlapping, showing the striking difference between the full concurrence and individual overlapping in dynamic double-slit for the electron entanglement.